Research article

Rituraj*, Meir Orenstein and Shanhui Fan*

Scattering of a single plasmon polariton by multiple atoms for in-plane control of light

https://doi.org/10.1515/nanoph-2020-0340
Received June 19, 2020; accepted August 11, 2020; published online August 28, 2020

Abstract: We study the interaction of a single photon in a surface plasmon polariton mode with multiple atoms. We propose a system of two atoms to achieve a tunable scattering from subscattering to superscattering regimes by changing the angle of the incident photon. We also demonstrate a perfect electromagnetically-induced transparency using two atoms with two-level structures. The proposed framework is efficiently scalable to a system with a large number of atoms and opens up the possibility of designing novel atom-based optical devices. We design an atomically thin parabolic mirror to focus single photons and form a quantum mirage in a cavity built from atoms.

Keywords: electromagnetically induced transparency; nanophotonics; plasmonics; quantum electrodynamics; scattering; waveguide QED.

1 Introduction

Photon–atom interaction is an important subject with considerable theoretical and practical interests [1–3]. With the development of nanotechnology it has now become possible to tailor this interaction by designing nanophotonic structures with unique optical properties as well as artificial atoms like a superconducting qubit, quantum dot or a Rydberg atom in a highly excited state [4–6]. In recent years there have been numerous studies investigating the coherent scattering of a few photon Fock states by an atom [7–16]. Most of these studies, however, are concerned with a single or a few atoms coupled to one dimensional (1D) continuum of photonic modes of the waveguide [7–14, 17]. It has been shown that a two-level atom coupled to a waveguide acts as a perfect reflector near the resonant frequency, despite its subwavelength size. Similarly, it has been shown that an atom exhibits a cross section much larger than its physical dimensions for single photon scattering in free space near the resonant frequency [16]. Unlike a 1D waveguide, higher dimensionality provides much richer opportunities of manipulating photons through careful geometric arrangement of atoms [18]. Still, very few works have been done regarding scattering of single photons in two (2D) or three dimensions (3D) by multiple atoms.

In a recent work, we presented a general model for the scattering of surface plasmon polariton (SPP) mode by a single atom (in general any two-level quantum system) without making the usual dipole approximation [15]. Since the coupling of the atom to the slow surface modes is much stronger than its coupling to the free space modes, the system essentially represents an atom interacting with a 2D photonic environment. In the current work, we further develop the formalism to compute the scattering properties for a more complicated scenario of multiple atoms coupled to a single photon in the SPP mode. The proposed model is general and includes all the multiple scattering events. The 2D setting with multiple atoms allows us to implement complex photon based quantum circuitry, and here we exemplify it by a few basic examples. We show that a system of two atoms can be tuned to exhibit either subscattering or superscattering by simply changing the photon angle of incidence. We also achieve a perfect atom cloaking with zero scattering at a certain frequency between the resonant frequency of the two atoms. This is different from the usual electromagnetically-induced transparency (EIT) which is based on interference between the transition paths in an atom with at least a three-level structure [1, 19–21]. We further explore the possibilities of designing novel atom-based optical devices to manipulate single photons and demonstrate multiple atoms based single photon focusing and the formation of quantum mirage in a 2D cavity like system.

***Corresponding authors: Rituraj and Shanhui Fan**, Electrical Engineering, Stanford University, Stanford, USA,
E-mail: rituraj@stanford.edu (Rituraj), shanhui@stanford.edu (S. Fan). https://orcid.org/0000-0002-7842-6808 (Rituraj)
Meir Orenstein, Electrical Engineering, Technion Israel Institute of Technology, Haifa, Israel

Open Access. © 2020 Rituraj et al., published by De Gruyter. This work is licensed under the Creative Commons Attribution 4.0 International License.

2 Mathematical formulation

Here, we develop the formalism for a system of N two-level atoms coupled to a single photon in 2D SPP mode. An atom–SPP system is shown schematically in Figure 1 for two atoms. The infinite 2D surface that supports the SPP mode (shown in green) is taken to be the $z = 0$ plane and the nth atom (represented by red cylinder), is placed at the coordinates $(\mathbf{r}_n \equiv (x_n, y_n), h_n)$. We assume that the atom is separated from the surface by vacuum, and the SPP mode is ideal without any propagation losses. In the Coulomb gauge, the SPP vector potential operator $\mathbf{A}(\mathbf{r}, z)$ in the upper half space $(z > 0)$ is given by:

$$\mathbf{A}(\mathbf{r},z) = \frac{1}{2\pi}\iint dk_x\, dk_y \underbrace{\sqrt{\frac{\hbar}{2L_{\mathbf{k}}\epsilon_0\omega_{\mathbf{k}}}}\left(i\hat{k} - \frac{k}{\kappa}\hat{z}\right)e^{-\kappa z}e^{i\mathbf{k}\cdot\mathbf{r}}}_{\mathbf{A}_{\mathbf{k}}(\mathbf{r},\,z)} a_{\mathbf{k}} + H.c, \quad (1)$$

where, $a_k, a_k^\dagger$ are the Bosonic annihilation and creation operators for the SPP mode satisfying the commutation $[a(\mathbf{k}), a^\dagger(\mathbf{k}')] = \delta^2(\mathbf{k} - \mathbf{k}')$, $\hbar$ is the reduced Planck's constant, ϵ_0 is the vacuum permittivity, $\kappa = \sqrt{k^2 - \omega_{\mathbf{k}}^2/c^2}$ is the spatial decay rate of the mode along z, $L_{\mathbf{k}}$ is the characteristic modal length given by $L_{\mathbf{k}} = (\kappa^2 + k^2)/\kappa^3$ and is derived through normalization consideration [22–25], $H.c$ stands for Hermitian conjugate. $\omega_{\mathbf{k}}$ is the SPP mode frequency at in-plane wavevector $\mathbf{k} \equiv (k_x, k_y)$, and could be well approximated by Eq. (2) for frequency close to the surface plasmon frequency ω_{sp}:

$$\omega_{\mathbf{k}} = \sqrt{\frac{1+\varepsilon_m}{\varepsilon_m}}ck \approx \frac{\omega_p}{\sqrt{2}}\left(1 - \frac{k_p^2}{8k^2}\right) = \omega_{sp} - \frac{\beta}{k^2}, \quad (2)$$

where, ϵ_m is the real dielectric constant of the metal given by the Drude model, ω_p is its plasma frequency, k_p is the free space wave-vector magnitude at frequency $\omega_p\,(= ck_p)$, c is the speed of light in vacuum [26–28].

We assume that the atoms couple only to the SPP mode and ignore coupling to the free-space electromagnetic modes.

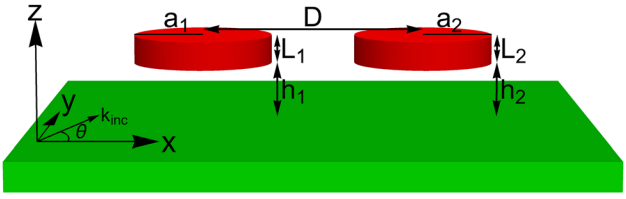

Figure 1: Two atoms (shown in red) coupled to the surface plasmon polariton (SPP) mode of an infinite two dimensional (2D) surface (shown in green). The surface is the $(z = 0)$ plane and each of the atom-like system confines the electron wave functions in a cylinder with radius a_n and height L_n, located at a distance h_n above the surface.

This assumption is well justified since the near field coupling to the SPP modes is much stronger than coupling to the free-space modes. It is also assumed that the atoms do not directly interact with each other. Starting with the standard minimal coupling Hamiltonian, for resonant coupling near the surface plasmon frequency, we can show that the light–matter interaction in the atom–SPP system can be described by the following spatial domain Hamiltonian [15]:

$$\begin{aligned} H =& \hbar\omega_{sp}\iint dx\, dy c^\dagger(\mathbf{r})c(\mathbf{r}) \\ &+ \hbar\beta\iint dx\, dy \iint dx'\, dy' \frac{\ln|\mathbf{r}-\mathbf{r}'|}{2\pi} c^\dagger(\mathbf{r})c(\mathbf{r}') \\ &+ \sum_{n=1}^{N} E_g^n b_g^{n\dagger} b_g^n + E_e^n b_e^{n\dagger} b_e^n + \sum_{n=1}^{N}\iint dx\, dy\Big(V_n(\mathbf{r})c^\dagger(\mathbf{r})b_g^{n\dagger}b_e^n \\ &+ V_n^*(\mathbf{r})c(\mathbf{r})b_e^{n\dagger}b_g^n\Big) \end{aligned} \quad (3)$$

where, E_g^n and E_e^n are the ground and excited state energies for the electron in the nth atom, and $b_g^n, b_g^{n\dagger}, b_e^n, b_e^{n\dagger}$ are the respective Fermionic annihilation and creation operators. $c(\mathbf{r}), c^\dagger(\mathbf{r})$ are the spatial Bosonic annihilation and creation operators respectively as defined by Eq. (4), and satisfy the commutation $[c(\mathbf{r}), c^\dagger(\mathbf{r}')] = \delta^2(\mathbf{r} - \mathbf{r}')$. $V_n(\mathbf{r})$ is the Fourier transform of the atom–field coupling strength $V_{\mathbf{k}}^n$ given by Eq. (5):

$$c(\mathbf{r}) = \frac{1}{2\pi}\iint dk_x\, dk_y\, e^{i\mathbf{k}\cdot\mathbf{r}}a_{\mathbf{k}}\ ;\ c^\dagger(\mathbf{r}) = \frac{1}{2\pi}\iint dk_x\, dk_y\, e^{-i\mathbf{k}\cdot\mathbf{r}}a_{\mathbf{k}}^\dagger \quad (4)$$

$$V_{\mathbf{k}}^{n*} = -\frac{e}{m}\langle e_n|\mathbf{A}_{\mathbf{k}}\cdot\mathbf{p}_n|g_n\rangle\ ;\ V_n(\mathbf{r}) = \frac{1}{2\pi}\iint dk_x\, dk_y\, e^{i\mathbf{k}\cdot\mathbf{r}}V_{\mathbf{k}}^n \quad (5)$$

where, e and m are respectively the charge and the rest mass of the electron, $\mathbf{p}_n = -i\hbar\vec{\nabla}_n$ is the canonical momentum operator for the electron in the nth atom. In the Hamiltonian of Eq. (3), we have ignored the terms related to intrinsic spin angular momentum and the $\mathbf{A}^2$ term. We have also made the usual rotating wave approximation in the interaction Hamiltonian [1, 2, 29]. These approximations are justified in the weak coupling regime (small $V_{\mathbf{k}}$), which is the case here and are also validated from the results shown later where the linewidths in scattering spectrum are much smaller than the resonant frequency. The logarithmic form in the second term of the Hamiltonian of Eq. (3) arises from the SPP dispersion relation in the short wavelength limit (Eq. (2)).

Consider an incident SPP photon with a wavevector $\mathbf{q}$ interacting with the atoms, the resulting stationary state can then be written as:

$$\begin{aligned} |\psi_{\mathbf{q}}\rangle =& \iint dx\, dy\, \phi(\mathbf{r})c^\dagger(\mathbf{r})\,|g, g, \ldots g, 0\rangle \\ &+ \sum_{n=1}^{N} e_{\mathbf{q}}^n\, b_e^{n\dagger}\, b_g^n\,|g, g, \ldots g, 0\rangle \end{aligned} \quad (6)$$

where, $|g, g, \ldots g, 0\rangle$ is the state with all atoms in the ground state and zero photons in the SPP mode, $\phi(\mathbf{r})$ is the photon field amplitude, and $e^n_{\mathbf{q}}$ is the excited state amplitude for the nth atom. Eq. (6) represents a complete basis for the system [7, 30]. Now, using Eq. (6) in the eigenvalue problem $H|\psi_{\mathbf{q}}\rangle = E_{\mathbf{q}}|\psi_{\mathbf{q}}\rangle$ gives the following equations:

$$\left(\hbar\omega_{sp} + \sum_{n=1}^{N} E_g^n - E_{\mathbf{q}}\right)\phi(\mathbf{r}) + \hbar\beta \iint dx'\, dy' \frac{\ln|\mathbf{r} - \mathbf{r}'|}{2\pi}\phi(\mathbf{r}') = -\sum_{n=1}^{N} e^n_{\mathbf{q}} V_n(\mathbf{r}) \quad (7)$$

$$(E_{\mathbf{q}} - E_e^n)e^n_{\mathbf{q}} = \iint dx\, dy\, V_n^*(\mathbf{r})\phi(\mathbf{r}). \quad (8)$$

Taking 2D Laplacian ($\hat{\Delta} \equiv \partial^2/\partial x^2 + \partial^2/\partial y^2$) of both sides of integral equation (7) and substituting $E_{\mathbf{q}} = \sum_n E_g^n + \hbar\omega_{sp} - \hbar\beta/q^2$, we get the 2D Helmholtz equation with N distributed source terms

$$\hat{\Delta}\phi(\mathbf{r}) + q^2\phi(\mathbf{r}) = -\frac{q^2}{\hbar\beta}\sum_{n=1}^{N} e^n_{\mathbf{q}}\hat{\Delta}V_n(\mathbf{r}). \quad (9)$$

Writing in dimensionless units by defining $\mathbf{r}' = k_{sp}\mathbf{r}$ and $\mathbf{q}' = \mathbf{q}/k_{sp}$, where $k_{sp} = \omega_{sp}/c$, we obtain

$$\hat{\Delta}'\left(\frac{\phi(\mathbf{r}')}{k_{sp}}\right) + q'^2\left(\frac{\phi(\mathbf{r}')}{k_{sp}}\right) = -q'^2\left(\frac{\omega_{sp}k_{sp}}{\beta}\right)\sum_{n=1}^{N} e^n_{\mathbf{q}'}\hat{\Delta}'\left(\frac{V_n(\mathbf{r}')}{\hbar\omega_{sp}k_{sp}}\right) \quad (10)$$

$$\frac{(E_{\mathbf{q}'} - E_e^n)}{\hbar\omega_{sp}}e_{\mathbf{q}'} = \iint dx'\, dy'\left(\frac{V_n^*(\mathbf{r}')}{\hbar\omega_{sp}k_{sp}}\right)\left(\frac{\phi(\mathbf{r}')}{k_{sp}}\right). \quad (11)$$

Following the standard procedure of computing scattering eigenstates, far away from the atoms where $V_n(\mathbf{r})$ approaches 0 fast enough as r increases, $\phi(\mathbf{r})$ could be expressed as a sum of incident and scattered waves [31]:

$$\phi(\mathbf{r}) = \phi_{inc} + \phi_{sca} = e^{i\mathbf{q}\cdot\mathbf{r}} + \phi_{sca}. \quad (12)$$

In Eq. (12), the incident wave ϕ_{inc} can be any SPP wave in the absence of coupling to the atoms ($V_n(\mathbf{r}) = 0$) and is taken here as a 2D SPP plane wave. The scattered wave ϕ_{sca} of the ensemble of atoms can be computed from the knowledge of the scattered fields for all the individual (isolated) atoms ϕ^n_{sca} ($1 \le n \le N$) [32–34]. The isolated atom scattering is computed by the procedure outlined in the previous work [15]. We model the two-level atom as an infinite cylindrical potential well as shown in Figure 1 with the following wavefunctions for the ground ($l_g = 1$) and excited ($l_e = 2$) states [35]:

$$\psi^n_{g,e}(\mathbf{r}, z) = \sqrt{\frac{2}{L_n}}\sin\frac{l_{g,e}\pi(z - h_n)}{L_n} \times \frac{\sqrt{2}}{aJ_1(j_0)}J_0(j_0|\mathbf{r} - \mathbf{r}_n|/a_n)\Theta_n(r, z) \quad (13)$$

where, J_n is the nth order Bessel function, j_0 is the first zero of the 0th order Bessel function, $\Theta_n(r, z)$ is a scalar function which is unity inside the cylinder ($|\mathbf{r} - \mathbf{r}_n| < a_n, h_n < z < h_n + L_n$) and zero outside. In this case, $V_n(\mathbf{r})$ has azimuthal symmetry (Eq. (5)) and the scattered field could be expressed in terms of the 0th order Hankel function of the first kind $H_0^{(1)}(q|\mathbf{r} - \mathbf{r}_n|)$.

$$\begin{aligned}\phi_n(\mathbf{r}) &= e^{i\mathbf{q}\cdot\mathbf{r}} + \phi^n_{sca} = e^{i\mathbf{q}\cdot\mathbf{r}_n}\left(e^{i\mathbf{q}\cdot(\mathbf{r}-\mathbf{r}_n)} + b_{0n}H_0^{(1)}(q|\mathbf{r} - \mathbf{r}_n|)\right)\\ &= e^{i\mathbf{q}\cdot\mathbf{r}_n}\left(\sum_{\substack{m=-\infty\\ m\neq 0}}^{\infty} i^m J_m(q|\mathbf{r} - \mathbf{r}_n|)e^{im\theta} + J_0(q|\mathbf{r} - \mathbf{r}_n|) + b_{0n}H_0^{(1)}(q|\mathbf{r} - \mathbf{r}_n|)\right)\end{aligned} \quad (14)$$

In the above expression for the total field $\phi_n(\mathbf{r})$, only the $m = 0$ angular momentum component of the incident wave is scattered and the scattering coefficient for the nth isolated atom b_{0n} is computed using appropriate boundary conditions as done in the previous work [15]. This procedure is repeated for all the atoms to determine $b_{0n}, \forall\, n \in \{1, \ldots, N\}$. It follows from the linearity of Eq. (10) that the scattered wave for the system of N atoms can be expressed as a superposition of the scattered waves by individual atoms as:

$$\phi(\mathbf{r}) = \phi_{inc} + \phi_{sca} = e^{i\mathbf{q}\cdot\mathbf{r}} + \sum_{n=1}^{N} b_n H_0^{(1)}(q|\mathbf{r} - \mathbf{r}_n|), \quad (15)$$

where, b_n is now the scattering coefficient for the nth atom, and is in general different from the isolated atom scattering coefficient b_{0n} due to multiple scattering between the different atoms. It can be shown that the above expression for the scattered field satisfies Eq. (10) in the far field where $V_n(\mathbf{r})$ goes to 0. To compute the scattering coefficients b_n, we use the Graf's addition theorem for the Hankel function (Eq. (16)) and express all the scattered waves $H_0^{(1)}(q|\mathbf{r} - \mathbf{r}_n|)$ in Eq. (15) in terms of Bessel functions centered at a particular jth atom.

$$H_0^{(1)}(q|\mathbf{r} - \mathbf{r}_n|) = \sum_{m=-\infty}^{\infty} H_m^{(1)}(q|\mathbf{r}_n - \mathbf{r}_j|)J_m(q|\mathbf{r} - \mathbf{r}_j|)e^{im\theta} \quad (16)$$

$$\begin{aligned}\phi(\mathbf{r}) &= e^{i\mathbf{q}\cdot\mathbf{r}} + b_j H_0^{(1)}(q|\mathbf{r} - \mathbf{r}_j|) + \sum_{\substack{n=1\\ n\neq j}}^{N}\sum_{m=-\infty}^{\infty} b_n H_m^{(1)}(q|\mathbf{r}_n - \mathbf{r}_j|)J_m(q|\mathbf{r} - \mathbf{r}_j|)e^{im\theta}\\ &= \sum_{m=-\infty}^{\infty} e^{im\theta}\left(i^m e^{i\mathbf{q}\cdot\mathbf{r}_j}J_m(q|\mathbf{r} - \mathbf{r}_j|) + \sum_{\substack{n=1\\ n\neq j}}^{N} b_n H_m^{(1)}(q|\mathbf{r}_n - \mathbf{r}_j|)J_m(q|\mathbf{r} - \mathbf{r}_j|)\right)\\ &\quad + b_j H_0^{(1)}(q|\mathbf{r} - \mathbf{r}_j|)\end{aligned} \quad (17)$$

The above expression can be interpreted as follows. The jth atom sees the combination of the incident plane wave and the waves scattered by all the other atoms as its total incident wave and only scatters the $m = 0$ angular momentum component. From linearity, the scattering coefficient b_j is proportional to the net amplitude of the $J_0(q|\mathbf{r} - \mathbf{r}_j|)$ term in Eq. (17) and the proportionality constant is the same as for that for the isolated atom in Eq. (14):

$$b_j = b_{0j}\left(e^{i\mathbf{q}\cdot\mathbf{r}_j} + \sum_{\substack{n=1 \\ n\neq j}}^{N} b_n H_m^{(1)}(q|\mathbf{r}_n - \mathbf{r}_j|)\right). \tag{18}$$

Repeating this for all the atoms ($j \in \{1, \ldots, N\}$), we obtain N linear equations which can be expressed as $\mathbf{Mb} = \mathbf{in}$, where $\mathbf{b} = (b_1, b_2, \ldots, b_N)^T, \mathbf{in} = (e^{i\mathbf{q}\cdot\mathbf{r}_1}, e^{i\mathbf{q}\cdot\mathbf{r}_2}, \ldots, e^{i\mathbf{q}\cdot\mathbf{r}_N})^T$ and $\mathbf{M}$ is a $N \times N$ matrix with elements $M_{m,n} = \delta_{m,n}/b_{0m} + (\delta_{m,n} - 1)H_0^{(1)}(q|\mathbf{r}_m - \mathbf{r}_n|)$. $\delta_{m,n}$ is the Kronecker delta function. Solving this system of linear equations then allows to treat the scattering from N atoms.

3 Results

Having presented a general framework to compute the scattering eigenstates of N atoms coupled to the 2D SPP mode, in this section we study a few interesting applications involving light manipulation using atoms.

3.1 Subscattering and superscattering

As the first case, we examine the interaction of a single SPP with two quantum dots with subwavelength horizontal separation. We choose the following parameters for the quantum dots: $a = 10\,\text{nm}$, $L = 3.35\,\text{nm}$, and they are separated by a distance $D = 260\,\text{nm}$ and placed at a height $h = 50\,\text{nm}$ from the surface as shown in Figure 1. For these values the atomic transition energy $\hbar\Omega_n = (E_e^n - E_g^n)$ lies close to the surface plasmon energy $\hbar\omega_{sp} = 0.1\,\text{eV}$. We choose for each atom a slightly different transition frequency amounting to different detuning values ($\Delta\omega_n = \Omega_n - \omega_{sp}, \hbar\Delta\omega_1 = -9.5\,\text{meV}, \hbar\Delta\omega_2 = -10\,\text{meV}$) which could be achieved either by choosing slightly different dimensions for the quantum dots or by applying static external fields. As shown in Figure 1, the angle of incidence is defined as the angle between the incident SPP wave vector $\mathbf{q}$ and the line joining the center of the two atoms (x axis). Figure 2 plots the total scattering cross section σ_T, given by Eq. (19), as a function of frequency for different angles of incidence θ [34].

$$\sigma_T = \frac{\lambda}{\pi^2}\int_0^{2\pi} d\phi |T(\phi)|^2 = \frac{2\lambda}{\pi}\left(|b_1|^2 + |b_2|^2 + 2J_0(qD)\text{Re}(b_1 b_2^*)\right) \tag{19}$$

The dotted blue curves in Figure 2a show the individual atomic scattering cross sections ($|b_{01}|^2, |b_{02}|^2$), while the red curves correspond to the total scattering cross section for the system of two atoms. The two detuning values are chosen such that their difference ($\Delta\omega_1 - \Delta\omega_2$) is smaller than the individual atomic linewidths resulting in a significant overlap between the two spectra (Figure 2a). As expected, we observe a highly anisotropic scattering behavior. For incidence angles close to the normal ($\theta = \pi/2$), the spectrum shows two peaks (Figure 2a and b). In a small frequency range between the peaks, we observe EIT-like behavior (subscattering) where the total scattering cross section is smaller than the individual scattering cross sections. At small angles of incidence, the spectrum shows only a single prominent resonant peak (Figure 2c and d). This is the typical signature of superscattering behavior where the total scattering cross section is larger than the individual ones. A classical analog of the current setup was considered in a previous work [36] where the authors used coupled mode theory formalism to analyze the transmission cross section of a metal film with two slits each supporting a localized resonance. The spectral response is characterized by two resonant modes: superradiant mode (the broad resonance in Figure 2a) and the subradiant mode (narrow resonance in Figure 2a). The two modes can also be computed as eigenmodes of the Hamiltonian of the

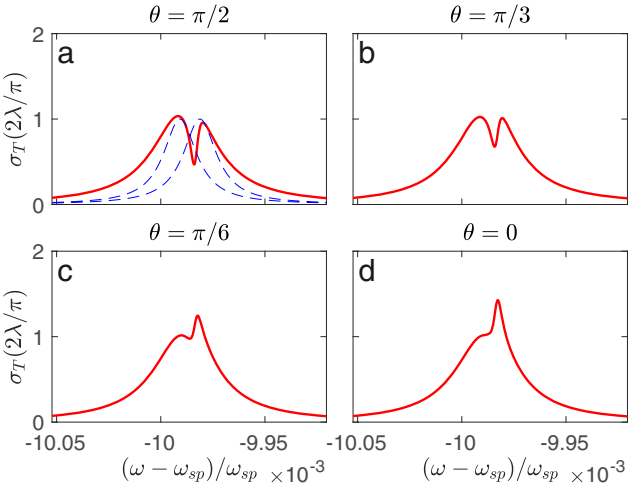

Figure 2: Scattering cross section of the system of two atoms coupled to the surface plasmon polariton (SPP) mode as shown in Figure 1, plotted as a function of frequency for different angles of incidence (plotted in red). The dotted blue curves show the scattering amplitudes ($|b_{0,1}|^2, |b_{0,2}|^2$) for the two individual atoms.

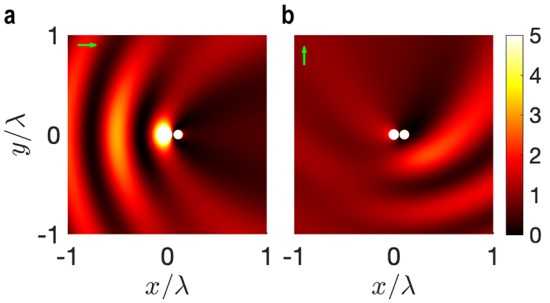

Figure 3: Total field intensity ($|\phi(\mathbf{r})|^2$) for an incident wave with frequency ($\omega - \omega_{sp} = -9.985 \times 10^{-3}\omega_{sp}$) and angle of incidence θ. (a) superscattering ($\theta = 0$), (b) subscattering ($\theta = \pi/2$). The green arrow indicates the direction of the incident plane wave.

system of two atoms after integrating out the photonic degree of freedom which introduces a coupling between the atoms. The EIT-like dip(superscattering) arises because of destructive(constructive) interference of radiation/scattering from the two resonances depending on the angle of incidence [16, 36–38]. The lateral inter-atom distance D is crucial for the required characteristic of the 2D scattering, since the radiation/scattering patterns from the two resonant modes will be very distinct for a large separation. Thus, EIT-like response is only observed for subwavelength separation where the overlap between the emission patterns can yield efficient destructive interference. The vertical separation $|h_1 - h_2|$ is less crucial, since it does not affect the overlap between the emission patterns and primarily controls the relative linewidth of the spectrum from the two atoms. Figure 3 shows the squared field amplitude $|\phi(\mathbf{r})|^2$ plot for two orthogonal directions of incidence at a frequency corresponding to the wavevector magnitude $q = 5.004\,k_{sp}$ or, wavelength $\lambda = 2.465\,\mu$m. We observe subscattering behavior at normal incidence and a superscattering behavior for grazing incidence. There is a high field amplitude concentrated near the two quantum dots which is more pronounced for the superscattering case as compared to the subscattering case.

3.2 Perfect atom cloaking

In the previous section, even though we observe an EIT-like behavior, the scattering cross section does not go to zero. One of the conditions required to obtain a perfect scattering cancellation for a system of two resonators as pointed out in Ref. [36] is to have identical radiation profile for the subradiant and superradiant eigenmodes or equivalently for the two resonators. It is possible to achieve this condition in our system, where the two atoms predominantly couple to the same 2D surface mode, by aligning them horizontally and displacing vertically as shown in Figure 4a. The two quantum dots are identical to those of the previous section ($a = 10\,$nm, $L = 3.35\,$nm) but with different detuning values ($\hbar\Delta\omega_1 = -0.15\,$meV, $\hbar\Delta\omega_2 = -0.16\,$meV) and ($h_1 = 200\,$nm, $h_2 = 250\,$nm). Similar to the previous case, these parameters are chosen such that the two individual atomic spectra have a significant overlap with slightly different resonant frequencies and linewidths. Here, since the system has azimuthal symmetry, only $m = 0$ angular momentum mode is scattered and the scattering is independent of angle of incidence. Figure 4b plots the scattering cross section as a function of frequency. The solid blue curve corresponds to the system of two atoms, whereas the dotted black curves correspond to the scattering spectrum of the individual atoms. We observe two peaks in the total scattering plot close to the two individual atomic resonances. In between the two peaks, at a certain frequency the scattering cross section goes to zero showing a perfect cloaking of the atoms. Furthermore we also see a broadening in the scattering linewidth evident from the broader tail in the blue spectrum where the net scattering cross section is larger than that of the individual atoms. The EIT-like spectrum is qualitatively similar to the one discussed in the previous subsection (Figure 2a) and arises from Fano interference between the two resonant pathways corresponding to the superradiant (broader peak in Figure 4b) and subradiant (narrow peak in Figure 4b) modes.

Figure 4c and d show the squared field amplitude ($|\phi(\mathbf{r})|^2$) plot for two different frequencies corresponding to perfect cloaking or EIT ($\sigma_T = 0$) and the higher frequency resonance ($\sigma_T = 2\lambda/\pi$) respectively. In the EIT case even though the scattered field is zero and field amplitude is constant far away from the atom, the near field amplitude is non-uniform. This is expected as the excited state amplitudes $e^n_{\mathbf{q}}$ for both the atoms is non-zero resulting in a net non-zero distributed source term in Eq. (10). At the EIT frequency, the emitted/scattered fields from the two source terms (atoms) cancel each other in the far field limit, and there is some energy stored in the near field and the excited state population. For the resonant scattering case shown in Figure 4d, we observe a large shadow behind the atoms and a large near field amplitude. This cloaking scheme is scalable and could be used to generate omnidirectional cloak for any distribution of atoms near a desired EIT frequency. It is also interesting to note that one can tune from an EIT-like response to Autler-Townes splitting (ATS) like behavior, which is characterized by a well separated doublet peak in spectral response, by introducing a direct (electronic) coupling between the two atoms [39–42].

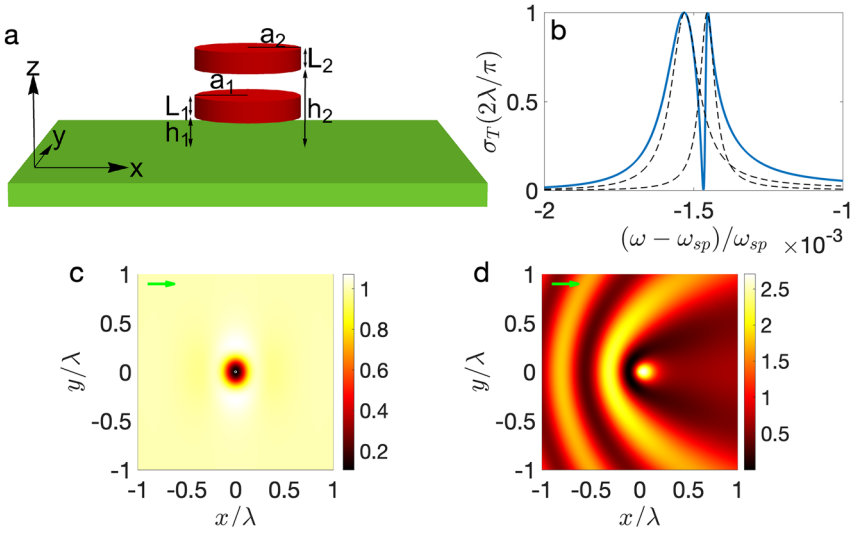

Figure 4: (a) The system of two horizontally aligned quantum dots coupled to the surface plasmon polariton (SPP) mode. (b) Scattering cross section ($|b_0|^2$) as a function of frequency. The solid blue curve corresponds to the system of two atoms and the dotted black curves are for the individual atoms. Total field intensity ($|\phi(\mathbf{r})|^2$) plot for (c) electromagnetically-induced transparency (EIT) ($\omega - \omega_{sp} = -1.5 \times 10^{-3}\omega_{sp}$), and (d) resonance ($\omega - \omega_{sp} = -1.4 \times 10^{-3}\omega_{sp}$). The green arrow indicates the direction of the incident wave.

3.3 Large structures

Having looked at the system of two atoms with sub-wavelength separation to achieve control and tuning of the scattering in the previous sections, now we design larger atomic optical devices to manipulate single photons in useful ways. In particular, we demonstrate an atomically thin parabolic mirror which concentrates light at its focus [43–46] and quantum mirage formation in an elliptical cavity like structure [47]. For the following computation, all the quantum dots are assumed to be identical with the same parameter values used in Section 3.1 and detuning $\hbar\Delta\omega = -9.5\,\text{meV}$.

Figure 5 shows the results for the parabolic mirror, with N identical atoms uniformly spaced along the parabola $y = -x^2/(4f)$, with $f = 50\lambda, \lambda = 2.46\,\mu\text{m}$. The incident plane wave is propagating along the axis of symmetry of the parabola (y axis). Figure 5a and b show the results for $N = 100$ atoms whereas Figure 5c and d correspond to $N = 1200$ atoms. Figure 5a and c show the total field amplitude squared $|\phi(\mathbf{r})|^2$ plot for the frequency corresponding to the atomic resonant frequency. The white dots represent the position of the atoms. We clearly see a high field amplitude concentrated near the focus of the parabola $\mathbf{f} = (0, -f)$. Furthermore, we observe a higher field amplitude in front of the mirror ($y < -x^2/(4f)$) and a much lower field behind it. The field amplitude at the focus and the contrast between the fields in front of and behind the mirror is greater for larger N as seen from Figure 5c. Thus the system acts as a parabolic mirror and the performance improves as the number of atoms N is increased. Also, from the inset in Figure 5c one can see that the focal spot size is smaller than a wavelength and is diffraction-limited [46]. When the atoms are more than a wavelength apart, the field amplitude at the focus increases almost linearly with N (intensity increases quadratically). Figure 5b and d show the bandwidth of the mirror and plot the maximum scattered field amplitude (normalized) near the focus of the parabola as a function of frequency (solid red curve). The dotted black curves correspond to the scattering coefficient for the individual atoms. For small N (Figure 5b), the separation between the atoms is large and the net interaction resulting from the multiple scattering between the atoms, is relatively weak resulting in a Lorentzian spectrum for the mirror which is quite similar to the scattering spectrum for individual atoms. As the number of atoms is increased (Figure 5d), the separation between the atoms decreases resulting in a stronger interaction. This leads to a much broader and frequency-shifted spectrum as observed in Figure 5d.

Finally, we discuss an interesting case of quantum mirage formation [47] for a system of 150 identical atoms uniformly spaced along the circumference of an ellipse ($x^2/a^2 + y^2/b^2 = 1$) with ($a = 5\lambda, b = 4\lambda$) and the wavelength corresponding to the individual atomic resonance ($\lambda = 2.46\,\mu\text{m}$). The atom to be imaged is placed at the positive focus of the ellipse ($\mathbf{f}_+ = (\sqrt{a^2 - b^2}, 0)$). Figure 6 shows the total field amplitude profile ($|\phi(\mathbf{r})|^2$) for an incident cylindrical wave of angular momentum $m = 0$, i.e., $\phi_{inc} = J_0(q|\mathbf{r} - \mathbf{f}_+|)$. The white dots show the position of the atoms. Besides observing a high field amplitude near the atom placed at the positive focus $\mathbf{f}_+$, we also observe a high field concentrated near the negative focus $-\mathbf{f}_+$ of the ellipse which is a mirage or optical image of the real atom. This results from a coherent superposition of the waves originally scattered by the atom at $\mathbf{f}_+$ and subsequently

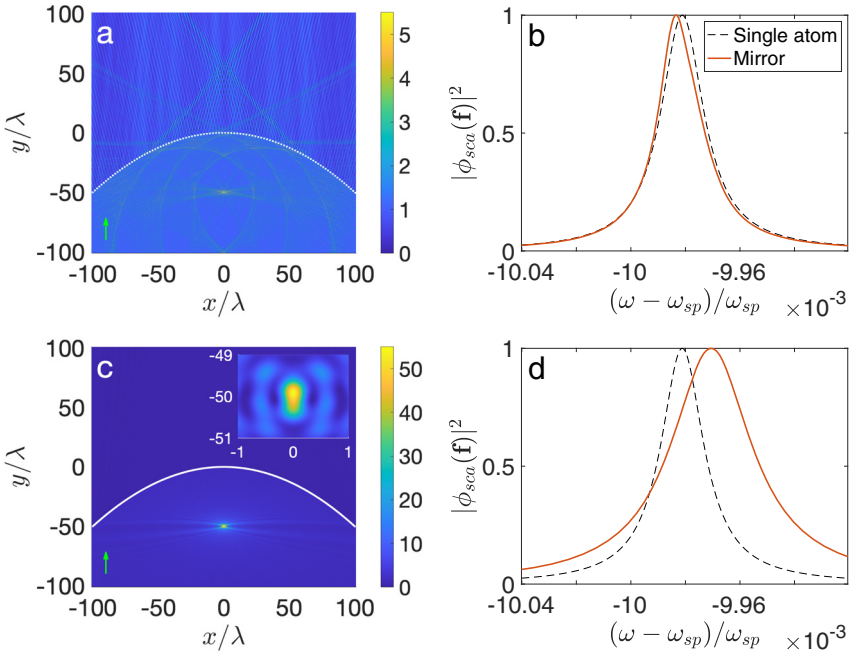

Figure 5: Total field intensity $(|\phi(\mathbf{r})|^2)$ plots for a system with (a) 100 atoms (marked by white dots), and (c) 1200 atoms, placed along a parabola. The green arrow indicates the direction of the incident wave. Maximum scattered field amplitude normalized and plotted in solid red as a function of frequency for (b) 100 atoms, and (d) 1200 atoms. The dotted black curve corresponds to the scattered field amplitude for a single atom.

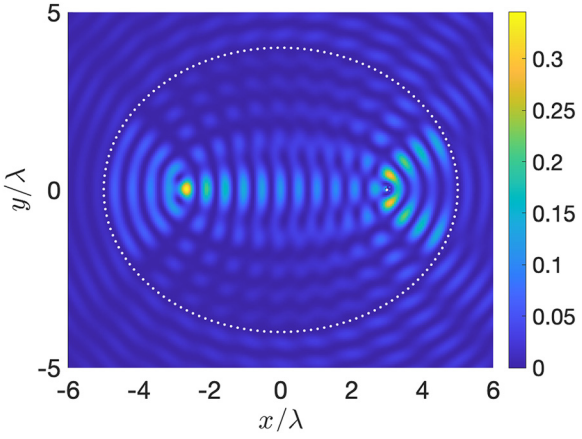

Figure 6: Total field intensity $(|\phi(\mathbf{r})|^2)$ plot for a system with 150 atoms (marked by white dots) placed along the circumference of an ellipse, and one atom at the positive focus of the ellipse. The incident wave is taken to be $\phi_{inc} = J_0(q|\mathbf{r} - \mathbf{f}_+|)$.

reflected by the atoms on the ellipse. This is because of the geometric property of the ellipse where the sum of distances of the two foci from any point on the ellipse is a constant $(2a)$. Note that we get a mirage only for a specific wavelength where the path difference $(\delta = 2a - 2|\mathbf{f}_+|)$ is an integral multiple of wavelength i.e., $q\delta = 2n\pi$ for some integer n.

4 Conclusion

We have demonstrated the possibility of realizing optical devices using multiple atoms interacting with a surface plasmon polariton. Such atomic structures are not only the smallest possible realization of optical structures but also offer unprecedented control over the optical response as compared to the conventional dielectric structures. Among various examples that we have shown, we have realized, for the first time, a perfect EIT for 2D SPP mode using only two-level atoms unlike the usual EIT which requires at least three-level quantum system. The proposed EIT scheme is general and could also be applied to cloak a large number of atoms.

Acknowledgment: This work is supported by a Vannevar Bush Faculty Fellowship from the U. S. Department of Defense (Grant No. N00014-17-1-3030). Rituraj acknowledges the support from a Stanford Graduate Fellowship.

Author contribution: All the authors have accepted responsibility for the entire content of this submitted manuscript and approved submission.

Research funding: This work is supported by a Vannevar Bush Faculty Fellowship from the U. S. Department of Defense (Grant No. N00014-17-1-3030).

Conflict of interest statement: The authors declare no conflicts of interest regarding this article.

References

[1] M. O. Scully and M. S. Zubairy, *Quantum Optics*, 1999.
[2] D. F. Walls and G. J. Milburn, *Quantum Optics*, Springer Science & Business Media, 2007.

[3] J. L. O'brien, A. Furusawa, and J. Vučković, "Photonic quantum technologies," *Nat. Photonics*, vol. 3, no. 12, p. 687, 2009.
[4] A. Goban, C. L. Hung, S. P. Yu, et al., "Atom–light interactions in photonic crystals," *Nat. Commun.*, vol. 5, p. 3808, 2014.
[5] A. F. Van Loo, A. Fedorov, K. Lalumiere, B. C. Sanders, A. Blais, and A. Wallraff, "Photon-mediated interactions between distant artificial atoms," *Science*, vol. 342, no. 6165, pp. 1494–1496, 2013.
[6] A. V. Gorshkov, J. Otterbach, M. Fleischhauer, T. Pohl, and M. D. Lukin, "Photon-photon interactions via Rydberg blockade," *Phys. Rev. Lett.*, vol. 107, no. 13, p. 133602, 2011.
[7] J. T. Shen and S. Fan, "Coherent photon transport from spontaneous emission in one-dimensional waveguides," *Opt. Lett.*, vol. 30, no. 15, pp. 2001–2003, 2005.
[8] J. T. Shen and S. Fan, "Coherent single photon transport in a one-dimensional waveguide coupled with superconducting quantum bits," *Phys. Rev. Lett.*, vol. 95, no. 21, p. 213001, 2005.
[9] S. Fan, Ş. E. Kocabaş, and J. T. Shen, "Input-output formalism for few-photon transport in one-dimensional nanophotonic waveguides coupled to a qubit," *Phys. Rev.*, vol. 82, no. 6, p. 063821, 2010,.
[10] P. Longo, P. Schmitteckert, and K. Busch, "Dynamics of photon transport through quantum impurities in dispersion-engineered one-dimensional systems," *J. Opt. Pure Appl. Opt.*, vol. 11, no. 11, p. 114009, 2009.
[11] L. Zhou, Z. R. Gong, Y. X. Liu, C. P. Sun, and F. Nori, "Controllable scattering of a single photon inside a one-dimensional resonator waveguide," *Phys. Rev. Lett.*, vol. 101, no. 10, p. 100501, 2008.
[12] J. Q. Liao, Z. R. Gong, L. Zhou, Y. X. Liu, C. P. Sun, and F. Nori, "Controlling the transport of single photons by tuning the frequency of either one or two cavities in an array of coupled cavities," *Phys. Rev.*, vol. 81, no. 4, p. 042304, 2010.
[13] D. Witthaut and A. S. Sørensen, "Photon scattering by a three-level emitter in a one-dimensional waveguide," *New J. Phys.*, vol. 12, no. 4, p. 043052, 2010.
[14] H. Zheng, D. J. Gauthier, and H. U. Baranger, "Waveguide-QED-based photonic quantum computation," *Phys. Rev. Lett.*, vol. 111, no. 9, p. 090502, 2013.
[15] M. O. Rituraj and S. Fan, "Two-level quantum system as a macroscopic scatterer for ultraconfined two-dimensional photonic modes," *Phys. Rev.*, vol. 102, no. 1, p. 013717, 2020.
[16] J. Liu, M. Zhou, and Z. Yu, "Quantum scattering theory of a single-photon Fock state in three-dimensional spaces," *Opt. Lett.*, vol. 41, no. 18, pp. 4166–4169, 2016.
[17] L. Zhou, H. Dong, Y. X. Liu, C. P. Sun, and F. Nori, "Quantum supercavity with atomic mirrors," *Phys. Rev.*, vol. 78, no. 6, p. 063827, 2008.
[18] E. Shahmoon, D. S. Wild, M. D. Lukin, and S. F. Yelin, "Cooperative resonances in light scattering from two-dimensional atomic arrays," *Phys. Rev. Lett.*, vol. 118, no. 11, p. 113601, 2017.
[19] S. E. Harris, J. E. Field, and A. Imamoğlu, "Nonlinear optical processes using electromagnetically induced transparency," *Phys. Rev. Lett.*, vol. 64, no. 10, p. 1107, 1990.
[20] K. J. Boller, A. Imamoğlu, and S. E. Harris, "Observation of electromagnetically induced transparency," *Phys. Rev. Lett.*, vol. 66, no. 20, p. 2593, 1991.
[21] M. Fleischhauer, A. Imamoğlu, and J. P. Marangos, "Electromagnetically induced transparency: Optics in coherent media," *Rev. Mod. Phys.*, vol. 77, no. 2, p. 633, 2005.
[22] K. J. Blow, R. Loudon, S. J. D. Phoenix, and T. J. Shepherd, "Continuum fields in quantum optics," *Phys. Rev.*, vol. 42, no. 7, p. 4102, 1990.
[23] B. A. Ferreira, B. Amorim, A. J. Chaves, and N. M. R. Peres, "Quantization of graphene plasmons," *Phys. Rev.*, vol. 101, no. 3, p. 033817, 2020.
[24] M. S. Tame, K. R. McEnery, Ş. K. Özdemir, J. Lee, S. A. Maier, and M. S. Kim, "Quantum plasmonics," *Nat. Phys.*, vol. 9, no. 6, pp. 329–340, 2013,.
[25] A. Archambault, F. Marquier, J. J. Greffet, and C. Arnold, "Quantum theory of spontaneous and stimulated emission of surface plasmons," *Phys. Rev. B*, vol. 82, no. 3, p. 035411, 2010.
[26] W. L. Barnes, A. Dereux, and T. W. Ebbesen, "Surface plasmon subwavelength optics," *Nature*, vol. 424, no. 6950, pp. 824–830, 2003.
[27] E. N. Economou, "Surface plasmons in thin films," *Phys. Rev.*, vol. 182, no. 2, p. 539, 1969.
[28] M. Jablan, M. Soljačić, and H. Buljan, "Plasmons in graphene: Fundamental properties and potential applications," *Proc. IEEE*, vol. 101, no. 7, pp. 1689–1704, 2013.
[29] E. A. Power and T. Thirunamachandran, "On the nature of the Hamiltonian for the interaction of radiation with atoms and molecules: (e/mc) p.a, - μ.e, and all that," *Am. J. Phys.*, vol. 46, no. 4, pp. 370–378, 1978.
[30] V. I. Yudson and P. Reineker, "Multiphoton scattering in a one-dimensional waveguide with resonant atoms," *Phys. Rev.*, vol. 78, no. 5, p. 052713, 2008.
[31] J. R. Taylor, *Scattering Theory: The Quantum Theory of Nonrelativistic Collisions*, Courier Corporation, 2006.
[32] G. O. Olaofe, "Scattering by an arbitrary configuration of parallel circular cylinders," *JOSA*, vol. 60, no. 9, pp. 1233–1236, 1970.
[33] D. Felbacq, G. Tayeb, and D. Maystre, "Scattering by a random set of parallel cylinders," *JOSA A*, vol. 11, no. 9, pp. 2526–2538, 1994.
[34] G. O. Olaofe, "Scattering by two cylinders," *Radio Sci.*, vol. 5, no. 11, pp. 1351–1360, 1970.
[35] A. S. Baltenkov and A. Z. Msezane, "Electronic quantum confinement in cylindrical potential well," *Eur. Phys. J. D*, vol. 70, no. 4, p. 81, 2016.
[36] L. Verslegers, Z. Yu, Z. Ruan, P. B. Catrysse, and S. Fan, "From electromagnetically induced transparency to superscattering with a single structure: A coupled-mode theory for doubly resonant structures," *Phys. Rev. Lett.*, vol. 108, no. 8, p. 083902, 2012.
[37] R. G. DeVoe and R. G. Brewer, "Observation of superradiant and subradiant spontaneous emission of two trapped ions," *Phys. Rev. Lett.*, vol. 76, no. 12, p. 2049, 1996.
[38] R. H. Dicke, "Coherence in spontaneous radiation processes," *Phys. Rev.*, vol. 93, no. 1, p. 99, 1954.
[39] S. H. Autler and C. H. Townes, "Stark effect in rapidly varying fields," *Phys. Rev.*, vol. 100, no. 2, p. 703, 1955.
[40] D. D. Smith, H. Chang, K. A. Fuller, A. T. Rosenberger, and R. W. Boyd, "Coupled-resonator-induced transparency," *Phys. Rev.*, vol. 69, no. 6, p. 063804, 2004.
[41] B. Peng, Ş. K. Özdemir, W. Chen, F. Nori, and L. Yang, "What is and what is not electromagnetically induced transparency in whispering-gallery microcavities," *Nat. Commun.*, vol. 5, no. 1, pp. 1–9, 2014,.

[42] P. Ginzburg and M. Orenstein, "Slow light and voltage control of group velocity in resonantly coupled quantum wells," *Opt. Express*, vol. 14, no. 25, pp. 12467–12472, 2006.
[43] A. Vakil and N. Engheta, "One-atom-thick reflectors for surface plasmon polariton surface waves on graphene," *Opt. Commun.*, vol. 285, no. 16, pp. 3428–3430, 2012.
[44] G. Alber, J. Z. Bernád, M. Stobińska, L. L. Sánchez-Soto, and G. Leuchs, "QED with a parabolic mirror," *Phys. Rev.*, vol. 88, no. 2, p. 023825, 2013.
[45] L. H. Ford and N. F. Svaiter, "Focusing vacuum fluctuations," *Phys. Rev.*, vol. 62, no. 6, p. 062105, 2000.
[46] P. N. Melentiev, A. A. Kuzin, D. V. Negrov, and V. I. Balykin, "Diffraction-limited focusing of plasmonic wave by a parabolic mirror," *Plasmonics*, vol. 13, no. 6, pp. 2361–2367, 2018.
[47] H. C. Manoharan, C. P. Lutz, and D. M. Eigler, "Quantum mirages formed by coherent projection of electronic structure," *Nature*, vol. 403, no. 6769, pp. 512–515, 2000.